Numerical simulation on Heat Extraction Performance of Enhanced Geothermal System under the Different Well layout

Abstract

China has hundreds of thousands of oil and water wells, about 30 percent of which have been abandoned currently. If we can convert abandoned wells into geothermal wells, it will save lots of money and reduce drilling and completion time greatly. In this paper, six enhanced geothermal system (EGS) well layout schemes are proposed based on the utilization of abandoned oil-water wells and common oilfield well pattern. Six common injection-production well pattern in oilfield are combined to hot dry rock (HDR) production and the heat extraction performance is simulated. The results show that the injection well number and the location of injection wells have critical influence on the heat extraction performance. Under the same total injection mass flow rate, the injection well number is the key factor and the fracture area is the secondary factor on heat extraction when the HDR energy is enough. For electricity generation, the life span is 20.2, 19.2, 19.0, 19.2, 18.2 and 13.9 years, the heat extraction ratio is 65.83, 57.35, 65.96, 62.79, 59.30 and 43.09 % from case 1 to case 6, respectively. For heating demand, the life span is 30.0, 30.0, 29.9, 30.0, 29.8, and 27.7 years, the heat extraction ratio is 78.91, 69.63, 77.02, 75.92, 72.27 and 58.94 % from case 1 to case 6, respectively. The total injection mass flow rate and injection temperature also have the negative effect on the heat extraction performance. Case 1 (row parallel well layout), Case 3 (four-spot well layout) and Case 4 (five-spot well layout) is the good choice both for electricity generation and heating demand. This study provides good guidance for the selection and optimization of different EGS well layout.

Keywords

Hot Dry Rock, Enhanced Geothermal System, Well layout, Abandoned oil-water wells, Thermal-Hydraulic model

Introduction

In recent years, with the increase of energy consumption and the intensification of greenhouse effect, clean energy plays an increasingly important role in the energy field (Ahmadi et al., 2018; Ramezanizadeh et al. 2019). Hot Dry Rock is a kind of deep geothermal resource which is clean renewable and widely distributed （Lu, 2018; Li et al., 2019; Wang et al., 2019）. Compared with solar, wind and tidal power, the exploitation of HDR is less affected by the environmental factors (Li et al., 2015; Zhang et al., 2019). EGS extracts heat from HDR reservoir through fluid injection and it is considered to be an important way to exploit HDR (Moya et al., 2018). Considering the environmental impacts and economic benefits, EGS is considered to be the best way for electricity generation (Xu et al., 2018). However, the establishment of EGS is a costly and complicated system engineering, reducing the cost and difficulty is an important way to accelerate the HDR development (Pan et al., 2018).

China has hundreds of thousands of oil and water wells, about 30 percent of which have been abandoned currently (Bu et al., 2012). If we can convert abandoned wells into geothermal wells, it will save lots of money and reduce drilling and completion time greatly (Caulk et al., 2017; Cheng et al., 2014; Davis et al., 2009). At the same time, the extracted heat can be used for oil exploitation and transportation and power supply for nearby oilfield (Kharseh et al., 2019). Moreover, there is a strong correlation between geothermal and oil-gas production. The data information of oil and gas exploration, drilling, completion and exploitation can be used for geothermal development and utilization (Nian et al., 2018; Yang et al., 2017). In this paper, six EGS well layout schemes are proposed based on the utilization of abandoned oil-water wells and common oilfield well pattern. Six common injection-production well pattern in oilfield are combined to HDR production and the heat extraction performance is simulated.

A proper selection of well layout may reduce the development cost and increase the heat extraction ratio (Ding et al., 2018; Li et al., 2018). The heat extraction performance of many kinds of well layout has been investigated currently. Yang et al. (2019) modeled the heat energy extraction performance in a triplet well layout and demonstrated that the well spacing, well radius, reservoir thickness and injection mass flow rate affect the heat extraction ratio significantly. Chen et al. (2017) simulated the heat extraction performance of doublet, triplet, quintuplet well layout and found that simply increasing the production well number is not necessary to improve the heat extraction performance of EGS, triplet well layout can perform better than quintuplet well layout or worse than an EGS with the standard doublet well layout. Xia et al. (2017) simulated horizontal doublet well layout which parallel injection and production wells connected by a set of single large wing fractures and proposed that 40 equidistant fractures along 1.2 km long parallel well section with well distance of 500 m would meet the industrial production-level system. There are many single-well geothermal systems, such as heat pipe single well (Huang et al., 2018), multilateral-well (Shi et al., 2019), tree-shaped wells (Liu et al., 2019), U-tube downhole (Lyu et al., 2018), and so on (Yan et al. 2019).

Although the previous simulation studies on heat extraction performance of different well layout are extensive, there is lack of a thorough and comprehensive comparison on heat extraction of application of oilfield injection scheme in HDR well layout. In this paper, the heat extraction performance of different well layout was investigated on the basis of the recovery and utilization of abandoned oil and water wells. Based on the injection scheme in oilfield, six ideal models for the HDR heat extraction are proposed. A thermal-hydraulic model is established to investigate the heat extraction performance of different well layout. Based on the model, the temperature distribution, pressure distribution, average production temperature, life span, average rock temperature and heat extraction ratio are proposed to evaluate the heat extraction performance of different well layout, the heat extraction performance of different well layout are compared, the effects of injection mass flow rate and injection temperature on the heat extraction performance are studied. This study provides good guidance for the selection and optimization of different EGS well layout.

Methodology

Model assumptions

In this work, we focus on the heat extraction performance of EGS under different combination of fracture and well array. The computational model includes the following assumptions:

(1) The HDR reservoir rock is homogenous and isotropic. The density, porosity, permeability, heat conductivity and heat capacity at constant pressure of HDR reservoir rock consider to be constant under the heat extraction condition. The HDR reservoir is saturated with water before the heat extraction operation.

(2) The water keeps in liquid state under the heat extraction condition, because the pressure and temperature meet the conditions of to keep it in liquid state (the specification of water phase diagram see **Figure 1.**). The density, dynamic viscosity, heat conductivity and heat capacity at constant pressure of water changes with temperature (see **Figure 2.** – **Figure 5.**).

(3) The permeability of the rock matrix is relatively lower, almost impermeable. Assuming there is a fracture between each injection well and production well as the key heat extraction channel. The fracture penetrates through the computational reservoir along corresponding the injection well and production well. The maximum distance among the injection well keeps consistent under different well layout. The reservoir descriptions of computational model are shown in **Table 2.**

Mathematical equations

The flow of water is laminar flow and subject to Darcy's law. Firstly, according to the mass conservation equation and Darcy law, the water flow in the porous media and the Darcy seepage velocity u can be described as (Liang et al., 2016)

$$\frac{\partial(\rho_{\mathrm{w}}\varepsilon_{\mathrm{p}})}{\partial t}+\nabla\cdot(\rho_{\mathrm{w}}u)=-Q_{\mathrm{m}} \tag{1}$$

$$u=-\frac{k}{\mu_{\mathrm{w}}}(\nabla p+\rho_{\mathrm{w}}g\nabla z) \tag{2}$$

where ρ_{w} denotes water density, ε_{p} denotes the rock matrix porosity, t denotes the time, ∇ denotes the Hamiltonian operator, u denotes the Darcy seepage velocity, Q_{m} denotes the source term, which is the mass transfer between the rock matrix and fractures, k denotes the rock matrix permeability, μ_{w} denotes water viscosity, p denotes the pressure and $\rho_{\mathrm{w}}g\nabla z$ denotes the gravity term.

The rock matrix is regarded as elastic porous storage and the effect of pressure on porosity is considered

$$\frac{\partial(\rho_{\mathrm{w}}\varepsilon_{\mathrm{p}})}{\partial t}=\varepsilon_{\mathrm{p}}\frac{\partial\rho_{\mathrm{w}}}{\partial t}+\rho_{\mathrm{w}}\frac{\partial\rho_{\mathrm{w}}}{\partial p}\frac{\partial p}{\partial t} \tag{3}$$

According to the state equation of the rock matrix, the rock compressibility can be described as

$$C_{\mathrm{m}} = \frac{1}{\varepsilon_{\mathrm{p}}}\frac{\partial \varepsilon_{\mathrm{p}}}{\partial p} \tag{4}$$

Define S as the storage coefficient of rock matrix and it can be described as

$$S = \varepsilon_{\mathrm{p}} C_{\mathrm{m}} \tag{5}$$

Substituting Equation (2)-(5) into (1), the seepage field equation of water in the porous media is obtained

$$\varepsilon_{\mathrm{p}}\frac{\partial \rho_{\mathrm{w}}}{\partial t} - \nabla \cdot \rho_{\mathrm{w}}\left[\frac{k}{\mu}(\nabla p + \rho_{\mathrm{w}} g \nabla z)\right] = -\rho_{\mathrm{w}} S \frac{\partial p}{\partial t} - Q_{\mathrm{m}} \tag{6}$$

Similarly, the seepage field equation of water in the fracture can be expressed as

$$d_{\mathrm{f}}\varepsilon_{\mathrm{f}}\frac{\partial \rho_{\mathrm{w}}}{\partial t} - \nabla_{\mathrm{T}} \cdot d_{\mathrm{f}}\rho_{\mathrm{w}}\left[\frac{k_{\mathrm{f}}}{\mu}(\nabla_{\mathrm{T}} p + \rho_{\mathrm{w}} g \nabla_{\mathrm{T}} z)\right] = -d_{\mathrm{f}}\rho_{\mathrm{w}} S_{\mathrm{f}} \frac{\partial p}{\partial t} + d_{\mathrm{f}} Q_{\mathrm{m}} \tag{7}$$

where d_{f} denotes the fracture aperture, ε_{f} denotes the fracture porosity, ∇_{T} denotes the gradient operator on the fracture's tangential plane, k_{f} denotes the fracture permeability and S_{f} denotes the storage coefficient of fracture.

From previous studies (Cao et al., 2016; Jiang et al., 2014), the local thermal equilibrium is applicable under the condition of the heat transfer coefficient and area is relatively large, the fracture aperture is relatively small. Therefore, in this work the local thermal equilibrium theory is adopted to investigate the temperature field.

According to the energy conservation equation, the heat transfer process in the porous media can be described as (Xu et al., 2015; Saeid et al., 2013)

$$(\rho C_{\mathrm{p}})_{\mathrm{eff}}\frac{\partial T}{\partial t} + \rho_{\mathrm{w}} C_{\mathrm{p,w}} u \cdot \nabla T - \nabla \cdot (\lambda_{\mathrm{eff}} \nabla T) = -Q_{\mathrm{m,E}} \tag{8}$$

where T denotes the temperature of porous media, $C_{\mathrm{p,w}}$ denotes the water specific heat, $Q_{\mathrm{m,E}}$ denotes the heat transfer between the porous media and fractures, $(\rho C_{\mathrm{p}})_{\mathrm{eff}}$ denotes the effective volumetric capacity, λ_{eff} denotes the effective thermal conductivity. According to the volume average model, $(\rho C_{\mathrm{p}})_{\mathrm{eff}}$ and λ_{eff} can be described as

$$(\rho C_{\mathrm{p}})_{\mathrm{eff}} = (1-\varepsilon_{\mathrm{p}})\rho_{\mathrm{s}} C_{\mathrm{p,s}} + \varepsilon_{\mathrm{p}} \rho_{\mathrm{w}} C_{\mathrm{p,w}} \tag{9}$$

$$\lambda_{\mathrm{eff}} = (1-\varepsilon_{\mathrm{p}})\lambda_{\mathrm{s}} + \varepsilon_{\mathrm{p}}\lambda_{\mathrm{w}} \tag{10}$$

where ρ_{s} denotes density of the rock matrix, $C_{\mathrm{p,s}}$ and $C_{\mathrm{p,w}}$ denote the specific heat of the rock matrix and water, λ_{s} and λ_{w} denote the thermal conductivity of the rock matrix and water, respectively.

Similarly, the heat transfer process in the fracture can be described as

$$d_{\mathrm{f}}(\rho C_{\mathrm{p}})_{\mathrm{eff}}\frac{\partial T}{\partial t}+d_{\mathrm{f}}\rho_{\mathrm{w}}C_{\mathrm{p,w}}u\cdot\nabla_{\mathrm{T}}T-\nabla_{\mathrm{T}}\cdot(d_{\mathrm{f}}\lambda_{\mathrm{eff}}\nabla T)=d_{\mathrm{f}}Q_{\mathrm{m,E}} \quad (11)$$

Model and parameters under different well layout

In this work, six ideal models are established for the HDR heat extraction according to the oil field well layout. The case 1 is row opposite well layout, two production wells in the middle of reservoir and four injection wells are located on opposite sides to the production well. The case 2 is row cross well layout, two production wells in the middle of reservoir and six injection wells cross with the production wells on both sides. The case3 is four-spot well layout, three injection wells are located at the apex of an equilateral triangle with a side length of 400m and the production well is located at the center of the triangle. The case 4 is five-spot well layout, four injection wells are located at the apex of a square with a side length of 400m and the production well is located at the center of the square. The case 5 is seven-spot well layout, six injection wells are located at the apex of the hexagon with a side length of 200m and the production well is located at the center of the hexagon. The case 6 is nine-spot well layout, eight injection wells are located at the apex and midpoint of the square with a side length of 400m and the production well is located at the center of the square. The six models differ greatly in well layout, but there are common points among different models. First, for each model, there is a fracture between each injection well and production well as the key heat extraction channel, and the fracture penetrates through the reservoir along corresponding the injection well and production well. Second, the maximum distance among the injection well keeps consistent under different well layout and the maximum distance is set as 400m in this work.

The schematic of different well array and the computational model are shown in **Figure 6.** and **Figure 7.** respectively. The specific spatial descriptions of computational model are shown in **Table 2**.

The computational model mentioned above is adopted to simulate the heat extraction process of different well layout. The specific initial and boundary conditions are shown as below:

(1) The HDR reservoir rock initial temperature at the top is 473.15 K. The temperature increases linearly with the depth and the geothermal gradient is 0.03 K/m. The initial temperature of other outer boundaries can be calculated by the initial temperature at the top and the geothermal gradient. The outer boundaries are set as thermal insulation.

(2) The HDR reservoir rock initial pressure at the top is 40 MPa. The pressure increases linearly with the depth and the pressure gradient is 0.005 MPa/m. The initial pressure of other outer boundaries can be calculated by the initial pressure at the top and the pressure gradient. Set production pressure to 30 MPa.

(3) The injection wells are set as inlet boundaries. The injection temperature is set as 293.15K and the injection mass flow rate is set as 120 kg/s. The production wells are set as outlet boundaries. The production pressure is set as 30 MPa.

The specific descriptions mentioned above can be seen in **Table 3**.

In order to guarantee the same simulation condition, adopting the same principle to mesh computational model under different well layout. All the domains adopt the free tetrahedral mesh. For the injection and production wells adopt the extra fine mesh and the maximum element size is 4m. The other domain adopts the fine mesh. The specific mesh descriptions of different well layout can be seen in **Table 4**. The mesh diagram of different well layout can be seen in **Figure 8.**, the legend represents the element size.

Results and Discussion

Temperature and pressure distribution

In this section, the heat extraction performance of different well layout is compared under the total injection rate is 120 kg/s. **Figure 9.** and **Figure 10.** illustrate the temperature and pressure distribution of different well layout at 30th year. It can be observed that the heat extraction ratio and thermal residual position is different from case 1 to case 6. The production pressure keeps at 30 MPa and the injection pressure is much higher than production well to guarantee the fluid flow.

Since the total injection mass flow rate is the same, it can be speculated that the difference in temperature and pressure distribution is mainly caused by the combination of different well layout and fractures.

The Darcy velocity field and pore pressure field on x-y plane of case 1 is shown in **Figure 11**. From **Figure 11.**, it is found that the streamline and pressure contour near injection and production well is much denser than the rest of region. It indicates that the vicinity of injection and production well have higher velocity gradient and pressure gradient. Moreover, the pressure contours near the injection and production well are concentric circles, concluding that the wells are essentially boundaries of uniform pressure.

Driven by the pressure difference, working fluid flow from the injection well, through the rock matrix and fractures into the production well, thus the HDR heat extraction process can be realized. Compare the **Figure 11.** (a) and **Figure 11.** (b), it is found that where the pressure gradient small, the fluid flow velocity is small, it indicates that the fluid flow velocity mainly depends on the pressure gradient. Compare the **Figure 11.** and **Figure 8.**, it is found that the thermal residual region of case 1 is where both the pressure gradient and the fluid flow velocity are small. The law is also applicable to case 2 – case 6 and the pressure contour and streamline of case 2 – case 6 is shown in **Figure 12. – Figure 16**. From above, it can be concluded that the injection well number and the location of injection wells have critical influence on the thermal extraction performance. It is necessary to choose proper well layout according to actual demand.

Average production temperature and life span

Figure17. demonstrates the average production temperature and life span of different well layout under the total injection mass flow rate is 120 kg/s. From **Figure 17.**, it is found that the average production temperature declines with the heat extraction time increases, and the decline trend is different under different well layout. In the first 17 years, the average production temperature of case 3 is higher than other well layout and after the 17th year, the average production temperature of case 1 is the highest. The average production temperature of case 6 is always the lowest.

For case 2 and case 3, the injection-production wells ratio is the same (both are three), the fracture area of case 2 is larger than that of case 3. In the first 19 years, the average temperature of case 3 is higher than that of case 2 and after the 20th year, the result is contrary. It can be speculated that the production temperature is related to the fracture area when the HDR energy is enough, the smaller the fracture area, the higher the average production temperature.

For case 3 and case 5, the production well number and fracture area are same, the injection well number is three and six, respectively. In the first 21 years, the average temperature of case 3 is higher than that of case 5 and after the 22th year, the average temperature is almost the same. It can be speculated that the production temperature is related to the injection well number when the HDR energy is enough, the fewer the injection well number, the higher the average production temperature.

In the first few years, the HDR energy is enough, it is found that the average production temperature is case 3, case 1, case 4, case 5, case 2 and case 6 from high to low, respectively. The injection well number is 3, 4, 4, 6, 6 and 8, respectively. The fracture area is 8.3×10^5, 5.0×10^5, 7.1×10^5, 8.3×10^5, 11.2×10^5 and 12.1×10^5 m^2, respectively. From the data above, it can be concluded that the injection well number is the key factor on the average production temperature. When the injection well number is the same, the fracture area plays an important role on the average production temperature. Both the injection well number and fracture area have a negative effect on the average production temperature.

The average production temperature determines the life span of the enhanced geothermal system (EGS). The production temperature should be greater than 378.51 and 323.15 K to meet the electricity generation and heating demand, respectively. For electricity generation, the life span is 20.2, 19.2, 19.0, 19.2, 18.2 and 13.9 years from case 1 to case 6, respectively. For heating demand, the life span is 30.0, 30.0, 29.9, 30.0, 29.8, and 27.7 years case 1 to case 6, respectively. Since the maximum calculation time is 30 years, there may be errors in the life span statics for heating demand.

Average rock temperature and heat extraction ratio

The production mass flow rate is often used as an evaluation criterion in previous studies and it can be calculated by the velocity integral of specific two-dimension region in 3D model. The calculation result is different with the different integral region. For a certain well layout, we can choose a specific integral region (always the partial fracture region) to calculate the production mass flow rate and use it as an evaluation criterion for sensitivity analysis. However, in this work, the heat extraction of different well layout is mainly compared, there is no identical integral region to choose, and the calculation results of the production mass flow rate with different integral region cannot be put in the same standard for comparison.

Therefore, other characteristic parameters should be found to evaluate the heat extraction process. The average rock temperature is a reliable characteristic parameter. The simulation model is an ideal model and ignore the energy consumption. The lower the average rock temperature is, the better the heat extraction effect is and the heat extraction ratio calculated by the average rock temperature is more accurate. The definition of the heat extraction ratio η is given by

$$\eta = \frac{\iiint_V \rho_s C_{p,s} (T_{r0} - T_r(t)) dv}{\iiint_V \rho_s C_{p,s} (T_{r0} - T_{in}) dv} \qquad (12)$$

where T_{r0} denotes the initial temperature of the porous matrix, $T_r(t)$ denotes the temperature at time instant, T_{in} denotes the injection temperature.

Figure 18. demonstrates the average rock temperature and heat extraction ratio during 30 years of different well layout under the total injection mass flow rate is 120 kg/s. From **Figure 18.**, it is found that the heat extraction ratio is case 3, case 1, case 4, case 5, case2 and case 6 from high to low in the first 25 years, respectively. The results of heat extraction ratio are consistent with the

average production temperature.

In the last 5 years, the heat extraction ratio is case 1, case 3, case 4, case 5, case2 and case 6 from high to low, respectively. The fracture area is 5.0×10^5, 8.3×10^5, 7.1×10^5, 8.3×10^5, 11.2×10^5 and 12.1×10^5 m^2, respectively. If the simulation time is prolonged to 40 years, the heat extraction ratio of case 4 may surpass that of case 3. Therefore, it can be concluded that the injection well number is the key factor and the fracture area is the secondary factor on heat extraction when the HDR energy is enough, the influence of the injection well number is weakened and the fracture area is the key factor when the HDR energy is not enough.

Figure 19. demonstrates the heat extraction ratio for (a) Electricity generation and (b) Heating demand of different well layout under the total injection mass flow rate is 120 kg/s. Under the simulation condition, for electricity generation, the heat extraction ratio is 65.83, 57.35, 65.96, 62.79, 59.30 and 43.09 % from case 1 to case 6, respectively. For heating demand, the heat extraction ratio is 78.91, 69.63, 77.02, 75.92, 72.27 and 58.94 %, respectively. Since the maximum calculation time is 30 years, there may be errors in the heat extraction statics for heating demand. Under the simulation condition, Case 1, Case 3 and Case 4 is the good choice both for electricity generation and heating demand.

Effect of injection mass flow rate

The simulation results above is calculated under the total injection mass flow rate is 120 kg/s, in this section, the injection mass flow rate of single well is set as 40 kg/s to compare the heat extraction process of different well layout.

Figure 20. demonstrates the average production temperature and heat extraction ratio of different well layout under the single well injection mass flow rate is 40 kg/s. From the **Figure 20.**, we can see that average production temperature is case 3, case 1, case 4, case 5, case 2 and case 6 from high to low, respectively. The total injection mass flow rate is 120, 160, 160, 180, 180, 320 kg/s, respectively. Under the same single well injection mass flow rate, the total injection mass flow rate depends on the injection well number, the more the injection wells, the lower the average production temperature and the shorter the time to reach a stable temperature. When the injection well number is the same, the fracture area plays an important role on the average production temperature. The larger the fracture area, the lower the average production temperature. The injection well number determines the average production temperature in the whole process.

Figure 21. demonstrates the heat extraction ratio for (a) Electricity generation and (b) Heating demand of different well layout under the single well injection mass flow rate is 40 kg/s. Under the simulation condition, for electricity generation, the life span and heat extraction ratio are 14.8, 8.2, 19.0, 14.1, 8.5, 4.6 years and 65.20, 53.40, 65.96, 62.31, 57.64, 40.50 % from case 1 to case 6, respectively. For heating demand, the life span and heat extraction ratio are 20.2, 19.2, 19.0, 19.2, 18.2, 13.9 years and 81.90, 69.13, 77.02, 77.28, 72.18 and 58.21 %, respectively. Since the maximum calculation time is 30 years, there may be errors in the heat extraction statics for heating demand.

From the static results above, it is found that the total injection mass flow rate has negative effect on the life span and heat extraction ratio for the same well layout. Under the simulation condition, Case 1, Case 3 and Case 4 is the good choice both for electricity generation and heating demand.

Effect of injection temperature

Figure 22. compares the average production temperature and heat extraction ratio under the injection temperature is 293.15 and 303.15 K. For case 1, when the injection temperature increases from 293.15 to 303.15 K, the life span for electricity generation is extended from 20.2 to 20.9 years and the heat extraction ratio decreased from 65.82 to 62.79. The same law can be found in case 2 to case 6, too. The higher the injection temperature, the lower the average production temperature and the heat extraction ratio. The low injection temperature is beneficial to the heat extraction for all the cases. The heat extraction ratio of Case1, Case 3 and Case 4 is greatly affected by the injection temperature.

Conclusions

In this paper, six EGS well layout schemes are proposed based on the utilization of abandoned oil-water wells and common oilfield well pattern. Six common injection-production well pattern in oilfield are combined to HDR production and the heat extraction performance is simulated. A thermal-hydraulic model is established to investigate the heat extraction performance of different well layout. Based on the model, the temperature distribution, pressure distribution, average production temperature, life span, average rock temperature and heat extraction ratio are proposed to evaluate the heat extraction performance of different well layout, the heat extraction performance of different well layout are compared, the effects of injection mass flow rate and injection temperature on the heat extraction performance are studied. In summary, the key points this work includes:

(1) Six ideal models for the HDR heat extraction are proposed based on the recovery and utilization of abandoned oil and water wells. The models are row opposite, row cross, four-spot, five-spot, seven-spot and nice-spot well layout from case 1 to case 6, respectively.

(2) The vicinity of injection and production well have higher velocity gradient and pressure gradient. The fluid flow velocity mainly depends on the pressure gradient and the thermal residual region is where both the pressure gradient and the fluid flow velocity are small. The injection well number and the location of injection wells have critical influence on the heat extraction performance. It is necessary to choose proper well layout according to actual demand.

(3) Under the same total injection mass flow rate, the injection well number is the key factor and the fracture area is the secondary factor on heat extraction when the HDR energy is enough, the influence of the injection well number is weakened and the fracture area is the key factor when the HDR energy is not enough. Both the injection well number and fracture area have a negative effect on the average production temperature. Under the same total injection mass flow rate, Case 1, Case 3 and Case 4 is the good choice both for electricity generation and heating demand. For electricity generation, the life span is 20.2, 19.2, 19.0, 19.2, 18.2 and 13.9 years, the heat extraction ratio is 65.83, 57.35, 65.96, 62.79, 59.30 and 43.09 % from case 1 to case 6, respectively. For heating demand, the life span is 30.0, 30.0, 29.9, 30.0, 29.8, and 27.7 years, the heat extraction ratio is 78.91, 69.63, 77.02, 75.92, 72.27 and 58.94 % from case 1 to case 6, respectively.

(4) Under the same single injection mass flow rate, the total injection mass flow rate depends on the injection well number, the more the injection wells, the lower the average production temperature and the shorter the time to reach a stable temperature. Under the same single well injection mass flow rate, Case 1, Case 3 and Case 4 is the good choice both for electricity

generation and heating demand. Under the same total injection mass flow rate, the higher the injection temperature, the lower the average production temperature and the heat extraction ratio. The heat extraction ratio of Case1, Case 3 and Case 4 is greatly affected by the injection temperature.

However, the hydraulic-mechanical couple is not taken into consideration in this paper, the heat extraction performance of six EGS well layout need further study in the future.

Acknowledgements

The authors wish to thank Prof Shibin Li.

Declaration of conflicting interests

The author(s) declared no potential conflicts of interest with respect to the research, authorship, and/ or publication of this article.

Funding

ORCID iD

Appendix

Case 1	Row opposite well layout
Case 2	Row cross well layout
Case 3	Four-spot well layout
Case 4	Five-spot well layout
Case 5	Seven-spot well layout
Case 6	Nine-spot well layout
C_m	Rock compressibility, Pa^{-1}
$C_{p,w}$	Water specific heat, J/(kg·K)
$C_{p,s}$	Rock matrix specific heat, J/(kg·K)
d_f	Fracture aperture, m
EGS	Enhanced Geothermal System

HDR	Hot Dry Rock
k	Rock matrix permeability, m^2
k_f	Fracture permeability, m^2
p	Pressure, Pa
Q_m	the mass transfer between the rock matrix and fractures
$Q_{m,E}$	the heat transfer between the porous media and fractures
S	Storage coefficient of rock matrix, Pa^{-1}
S_f	Storage coefficient of fracture, Pa^{-1}
t	Time, s
T	Temperature of porous media, K
T_{in}	Injection temperature, K
T_p	Average production temperature, K
T_r	Average rock temperature, K
T_{ro}	Initial temperature of the porous matrix, K
u	Darcy seepage velocity, m/s
ρ_s	Rock matrix density, kg/m^3
ρ_w	Water density, kg/m^3
$(\rho C_p)_{eff}$	Effective volumetric capacity,
μ_w	Water viscosity, Pa·s
ε_f	Fracture porosity, %
ε_p	Rock matrix porosity, %
∇	Hamiltonian operator
∇_T	gradient operator on the fracture's tangential plane
λ_{eff}	Effective thermal conductivity, W/(m·K)
λ_s	Thermal conductivity of rock matrix, W/(m·K)
λ_w	Thermal conductivity of water, W/(m·K)
η	Heat extraction ratio, %

References

Ahmadi M H, Ghazvini M, Sadeghzadeh M, et al. (2018) Solar power technology for electricity generation: a critical review. *Energy Science & Engineering* 6(5): 340-361.

Ramezanizadeh M, Nazari M A, Ahmadi M H, et al. (2019) A review on the approaches applied for cooling fuel cells. *International Journal of Heat and Mass Transfer* 139: 517-525.

Bu X, Ma W and Li H (2012) Geothermal energy production utilizing abandoned oil and gas wells. *Renewable Energy* 41: 80-85.

Cao W, Huang W and Jiang F (2016) A novel thermal–hydraulic–mechanical model for the enhanced geothermal system heat extraction. *International Journal of Heat and Mass Transfer* 100: 661-671.

Caulk RA and Tomac I (2017) Reuse of abandoned oil and gas wells for geothermal energy production. *Renewable Energy* 112: 388-397.

Chen J and Jiang F (2015) Designing multi-well layout for enhanced geothermal system to better exploit hot dry rock geothermal energy. *Renewable Energy* 74: 37-48.

Cheng W, Li T, Nian Y, et al. (2014) Evaluation of working fluids for geothermal power generation from abandoned oil wells. *Applied Energy* 118: 238-245.

Davis AP and Michaelides EE (2009) Geothermal power production from abandoned oil wells. *Energy* 34: 866-872.

Ding J and Wang S (2018) 2D modeling of well array operating enhanced geothermal system. *Energy* 162: 918-932.

Huang W, Cao W and Jiang F (2018) A novel single-well geothermal system for hot dry rock geothermal energy exploitation. *Energy* 162: 630-644.

Jiang F, Chen J, Huang W et al. (2014) A three-dimensional transient model for EGS subsurface thermo-hydraulic process. *Energy* 72: 300-310.

Kharseh M, Al-Khawaja M and Hassani F (2019) Optimal utilization of geothermal heat from abandoned oil wells for power generation. *Applied Thermal Engineering* 153: 536-542.

Li K, Bian H, Liu C, et al. (2015) Comparison of geothermal with solar and wind power generation systems. *Renewable and Sustainable Energy Reviews*. 42: 1464-1474.

Li S, Xu T, Zhang S, et al. (2019) Hot dry rock geothermal resource potential in the Wudalianchi volcanic field, NE CHINA: Implications from geophysical exploration. *Energy Exploration & Exploitation* 37(2): 663-676.

Li X, and Zhu D (2018) Temperature Behavior During Multistage Fracture Treatments in Horizontal Wells. *Society Petroleum Engineering* 33: 522-538.

Liang B, Jiang H, Li J, et al. (2016) A systematic study of fracture parameters effect on fracture network permeability based on discrete-fracture model employing Finite Element Analyses. *Journal of Natural Gas Science and Engineering* 28: 711-722.

Liu Y, Wang G, Yue G, et al. (2019) Comparison of enhanced geothermal system with water and CO_2 as working fluid: A case study in Zhacanggou, Northeastern Tibet, China. *Energy Exploration & Exploitation* 37(2): 736-755.

Lu S-M (2018) A global review of enhanced geothermal system (EGS). *Renewable and Sustainable Energy Reviews* 81: 2902-2921.

Lyu Z, Song X, Li G, et al. (2018) Numerical analysis of characteristics of a single U-tube downhole heat exchanger in a geothermal well. *Geothermics* 72: 15-23.

Moya D, Aldás C and Kaparaju P (2018) Geothermal energy: Power plant technology and direct heat applications. *Renewable and Sustainable Energy Reviews* 94: 889-901.

Nian Y and Cheng W (2018) Evaluation of geothermal heating from abandoned oil wells. *Energy* 142: 592-607.

Pan S, Gao M, Shah KJ, et al. (2019) Establishment of enhanced geothermal energy utilization plans: Barriers and strategies. *Renewable Energy* 132: 19-32.

Saeid S, Al-Khoury R and Barends F (2013) An efficient computational model for deep low-enthalpy geothermal systems. *Computers & geosciences* 51: 400-409.

Shi Y, Song X, Wang G, et al. (2019) Numerical study on heat extraction performance of a multilateral-well enhanced geothermal system considering complex hydraulic and natural fractures. *Renewable Energy* 141: 950-963.

Wang Z, Jiang G, Zhang C, et al. (2019) Thermal regime of the lithosphere and geothermal potential in Xiong'an New Area. *Energy Exploration & Exploitation* 37(2): 787-810.

Xia Y, Plummer M, Mattson E, et al. (2017) Design, modeling, and evaluation of a doublet heat extraction model in enhanced geothermal systems. *Renewable Energy* 105: 232-47.

Xu C, Dowd P A and Tian Z F (2015) A simplified coupled hydro-thermal model for enhanced geothermal systems. *Applied Energy* 140: 135-145.

Xu T, Yuan Y, Jia X, et al. (2018) Prospects of power generation from an enhanced geothermal system by water circulation through two horizontal wells: A case study in the Gonghe Basin, Qinghai Province, China. *Energy* 148: 196-207.

Yang SY and Yeh HD (2009) Modeling heat extraction from hot dry rock in a multi-well system. *Applied Thermal Engineering* 29: 1676-1681.

Yan X, Liu Y, Wang G, et al. (2019) Optimal injection rate of water in the Guide Basin hot dry rock mining project. *Energy Exploration & Exploitation* 37(2): 721-735.

Yang Y, Huo Y, Xia W, et al. (2017) Construction and preliminary test of a geothermal ORC system using geothermal resource from abandoned oil wells in the Huabei oilfield of China. *Energy* 140: 633-645.

Zhang L, Ji H, Chen L, et al. (2019) Characteristics of geothermal reservoirs in the Wumishan Formation and groundwater of the Middle-Upper Proterozoic and the geothermal status in the Beijing–Tianjin–Hebei region: Implications for geothermal resources exploration. *Energy Exploration & Exploitation* 37(2): 811-833.

Figure captions

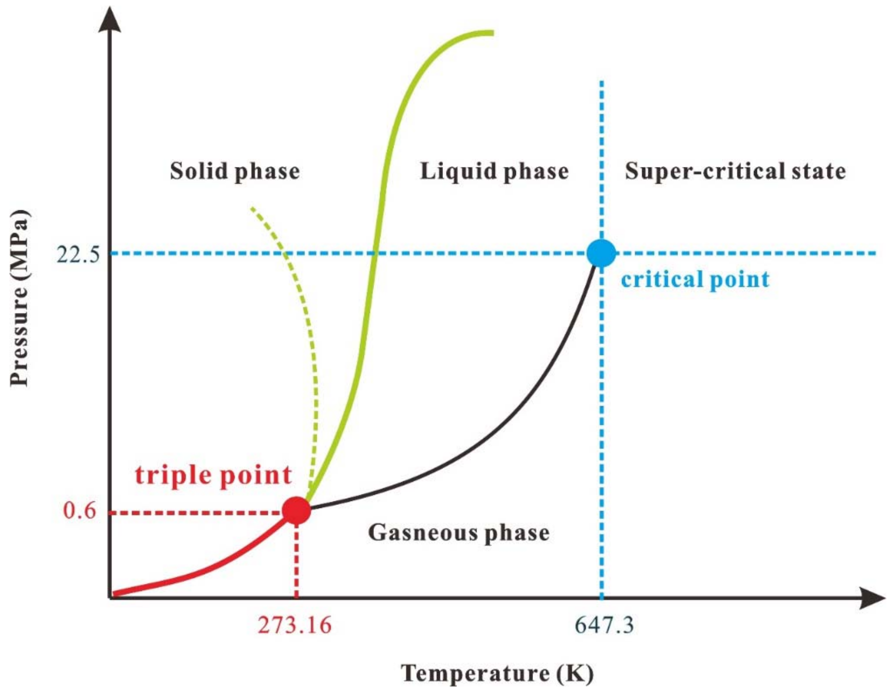

Figure 1. The pressure-temperature phase diagram of water

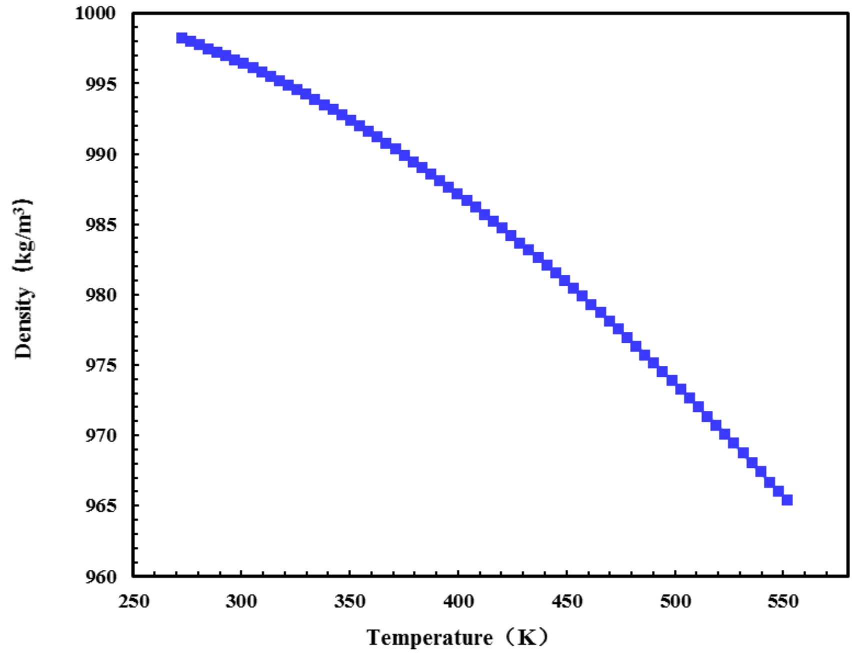

Figure 2. Variation curve of water density with temperature

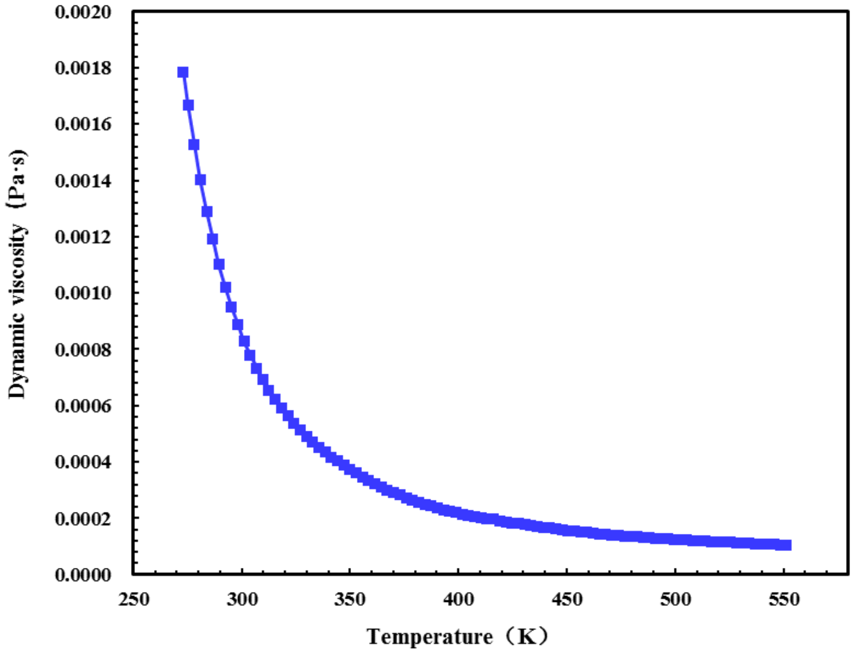

Figure 3. Variation curve of water dynamic viscosity with temperature

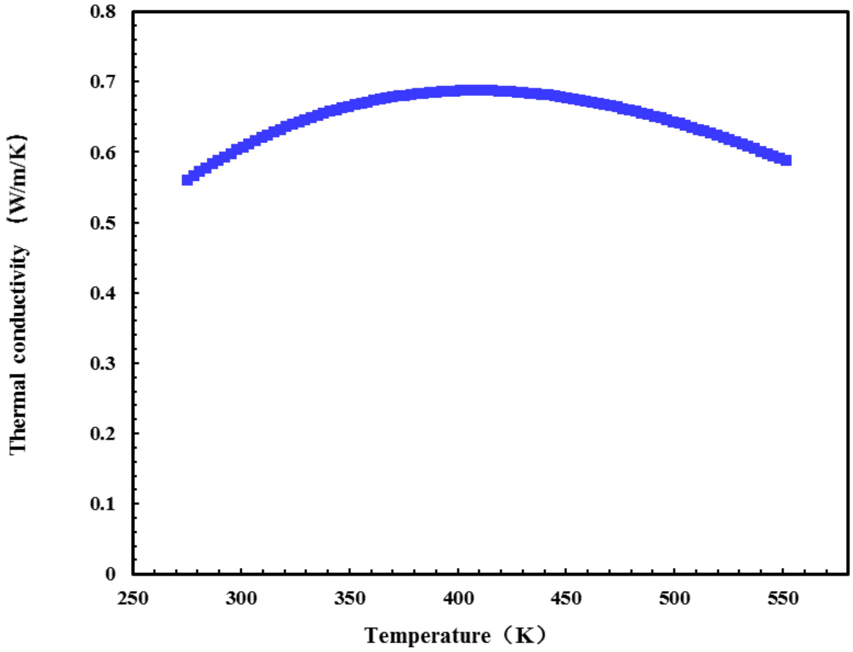

Figure 4. Variation curve of water thermal conductivity with temperature

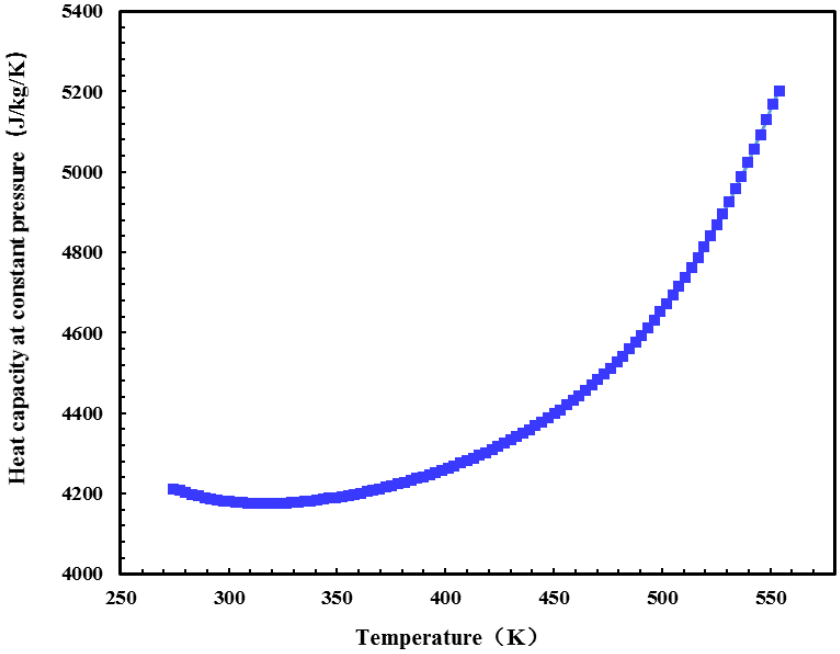

Figure 5. Variation curve of water heat capacity at constant pressure with temperature

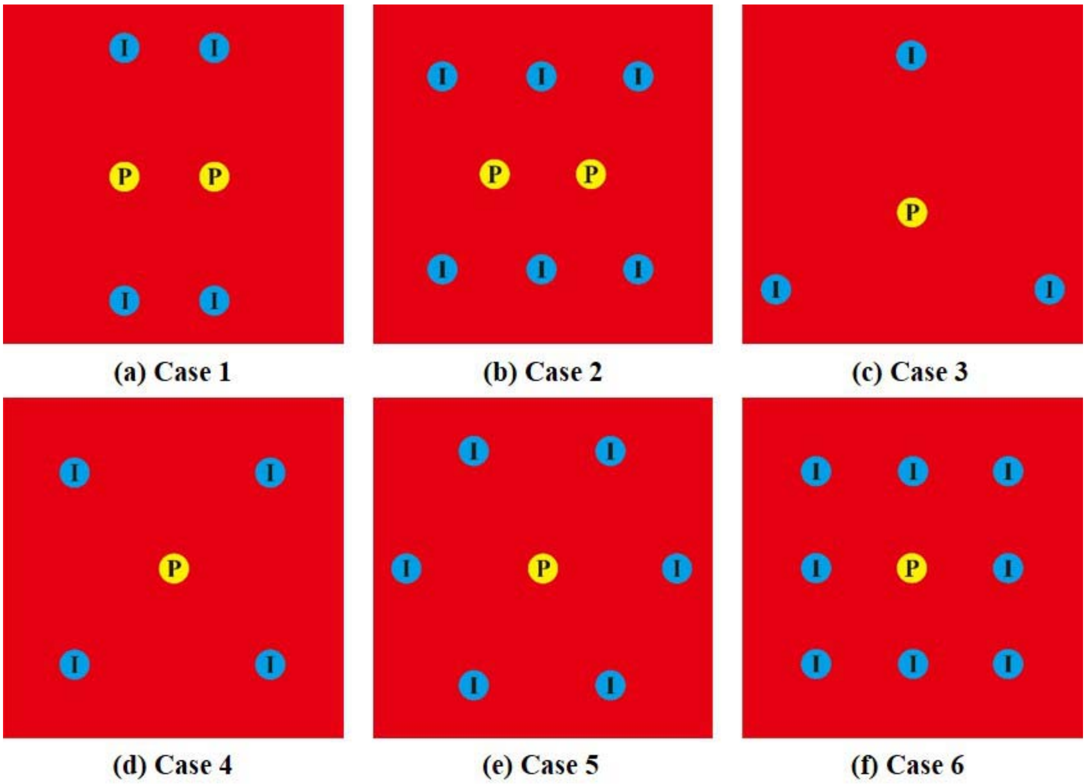

Figure 6. Schematic of different well array

Note: in the Figure 6, the red area represents HDR reservoir, the blue circles represent injection wells and the yellow circle represent production wells.

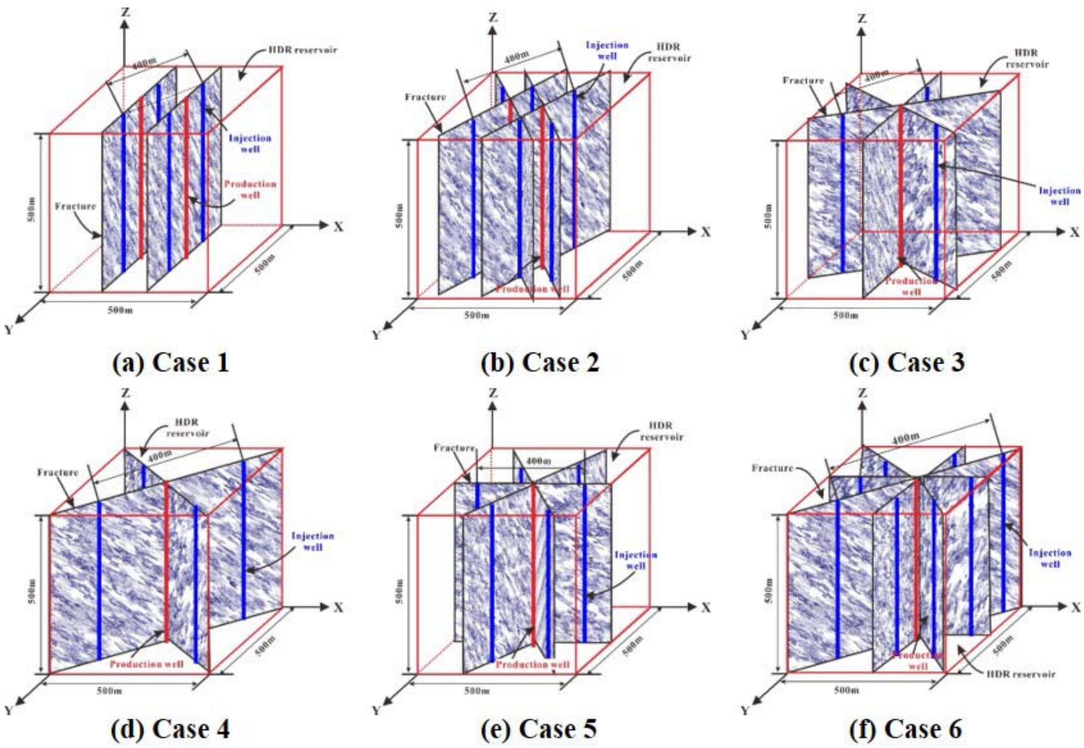

Figure 7. Schematic of the computational model

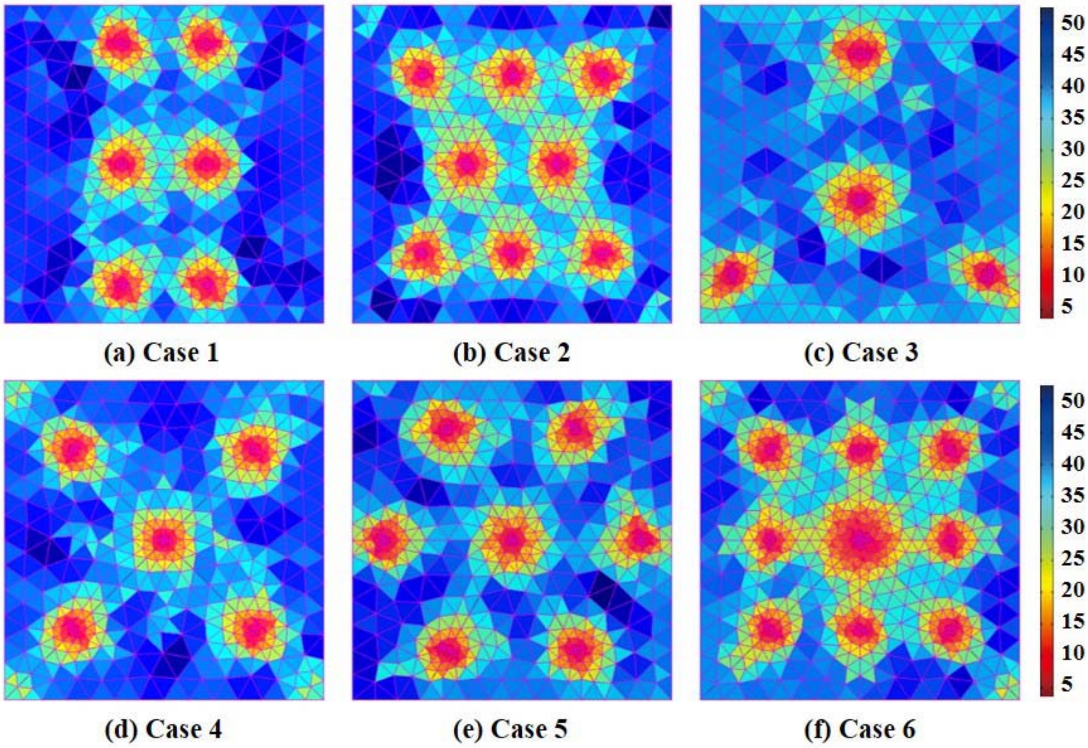

Figure 8. Mesh diagram of different well layout

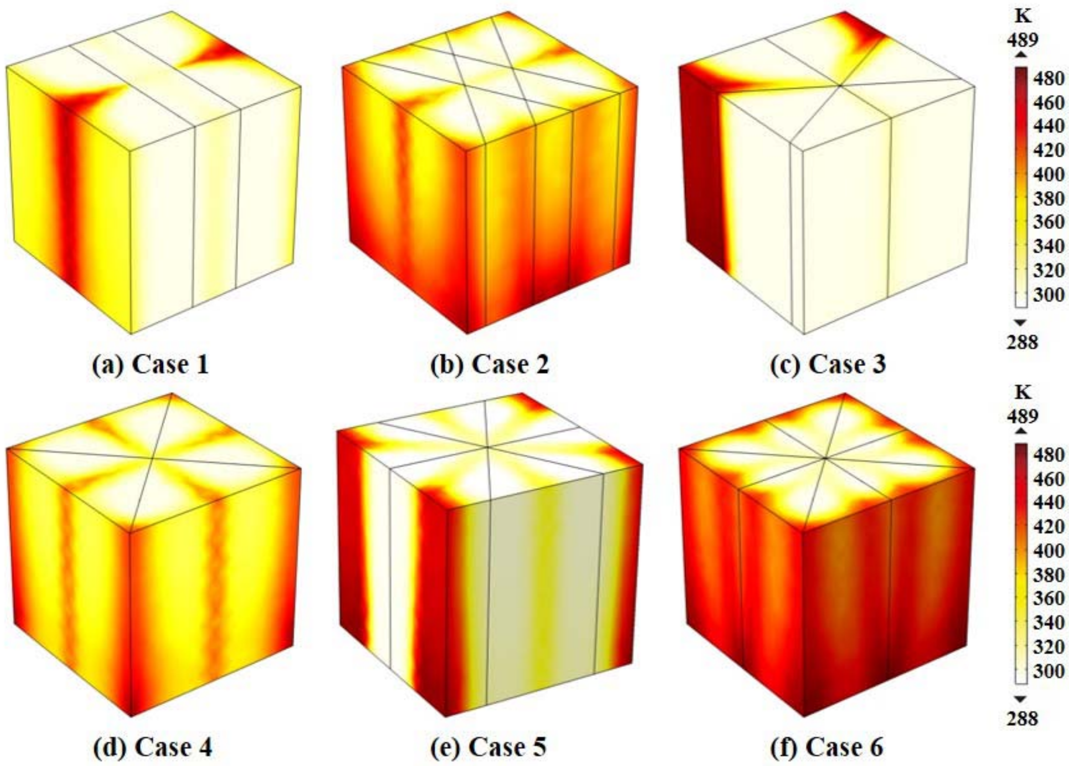

Figure 9. Temperature distribution of different well layout in the 30th year

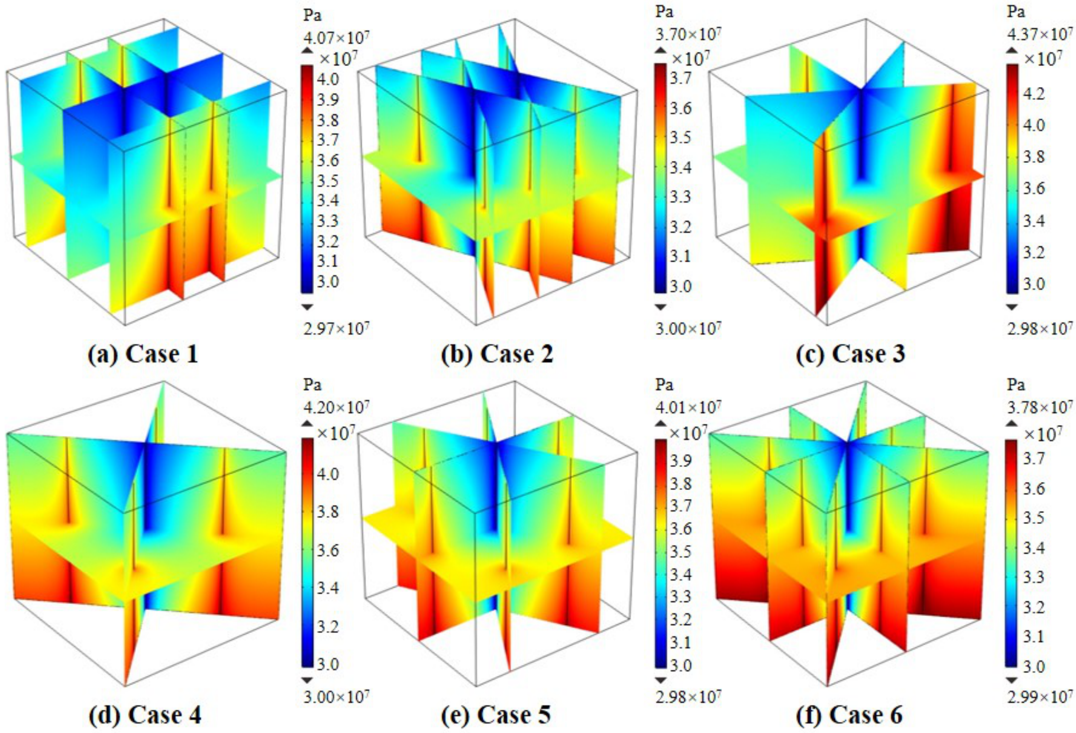

Figure 10. Pressure distribution of different well layout in the 30th year

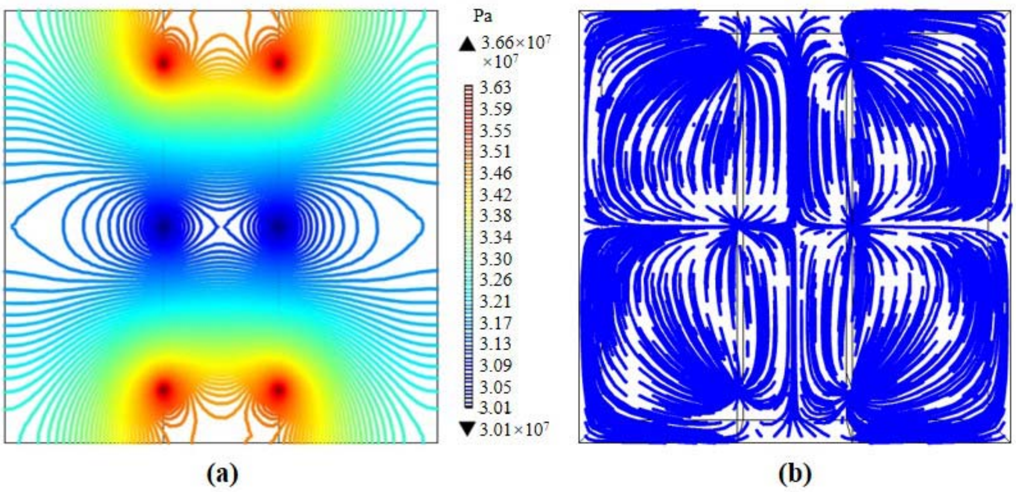

Figure 11. (a) Pressure contour; **(b)** Streamline of Case 1 in the 30th year

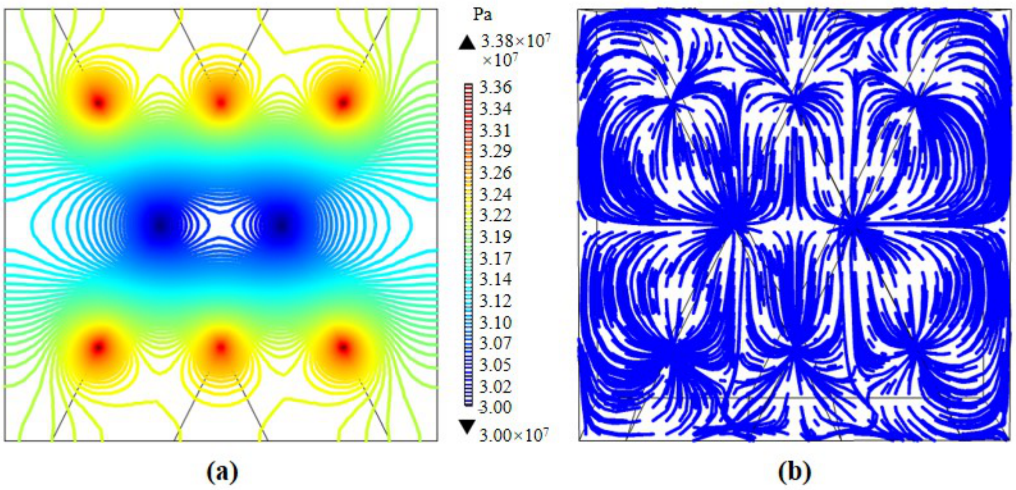

Figure 12. (a) Pressure contour; **(b)** Streamline of Case 2 in the 30th year

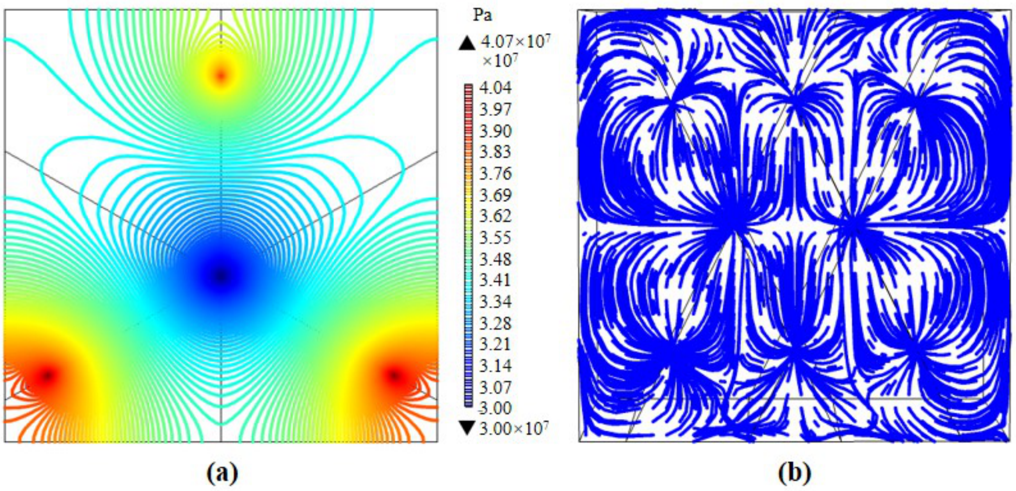

Figure 13. (a) Pressure contour; **(b)** Streamline of Case 3 in the 30th year

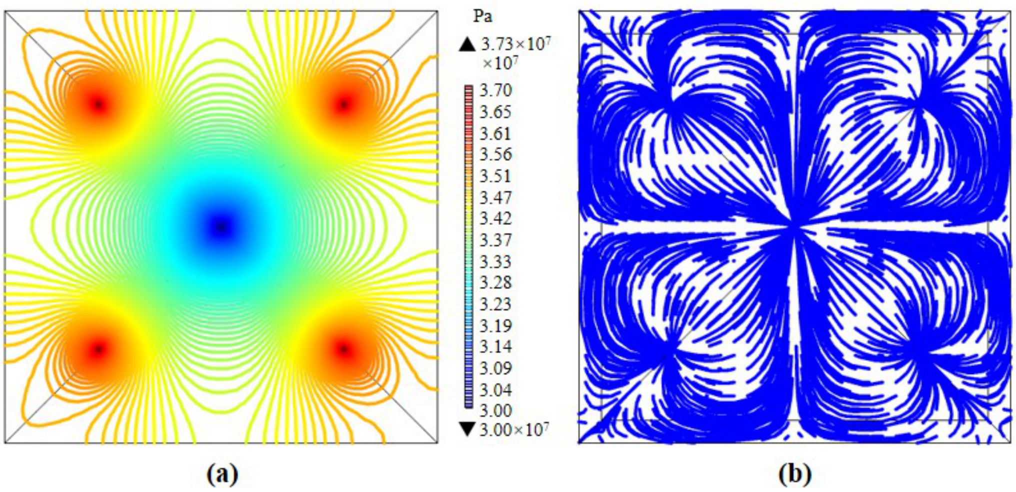

Figure 14. (a) Pressure contour; **(b)** Streamline of Case 4 in the 30th year

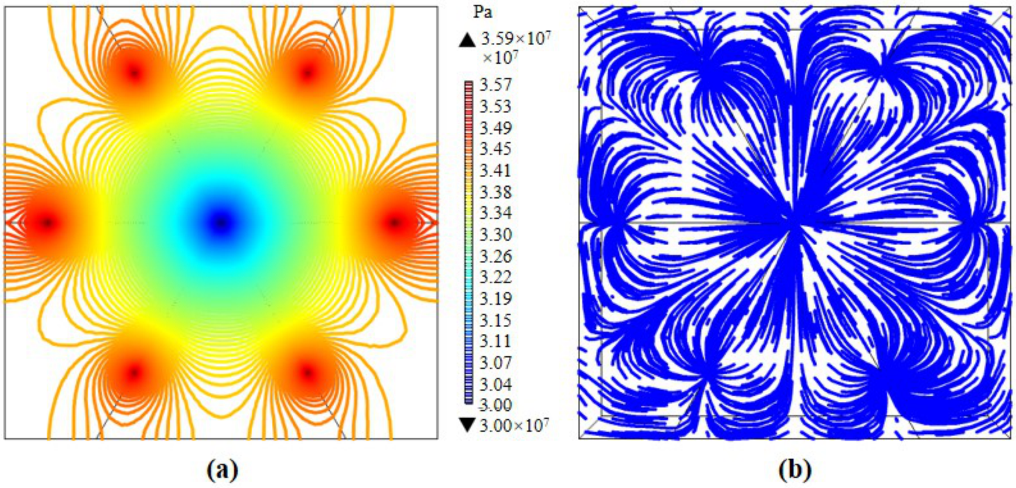

Figure 15. (a) Pressure contour; **(b)** Streamline of Case 5 in the 30th year

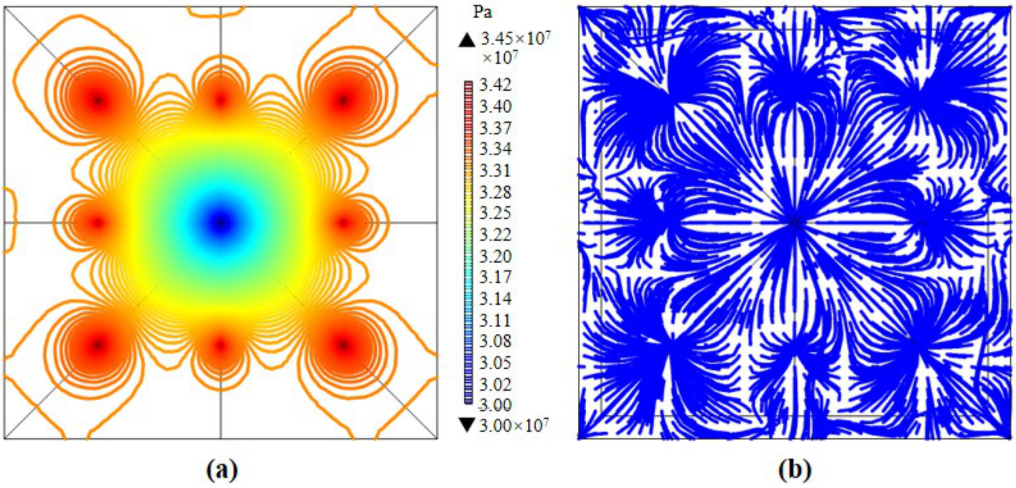

Figure 16. (a) Pressure contour; **(b)** Streamline of Case 6 in the 30th year

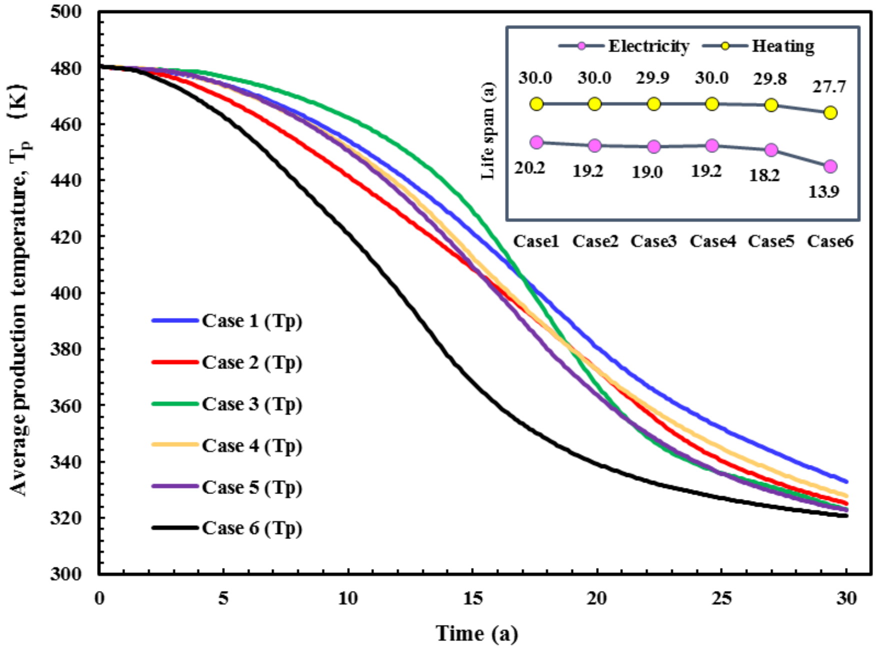

Figure 17. Average production temperature and life span

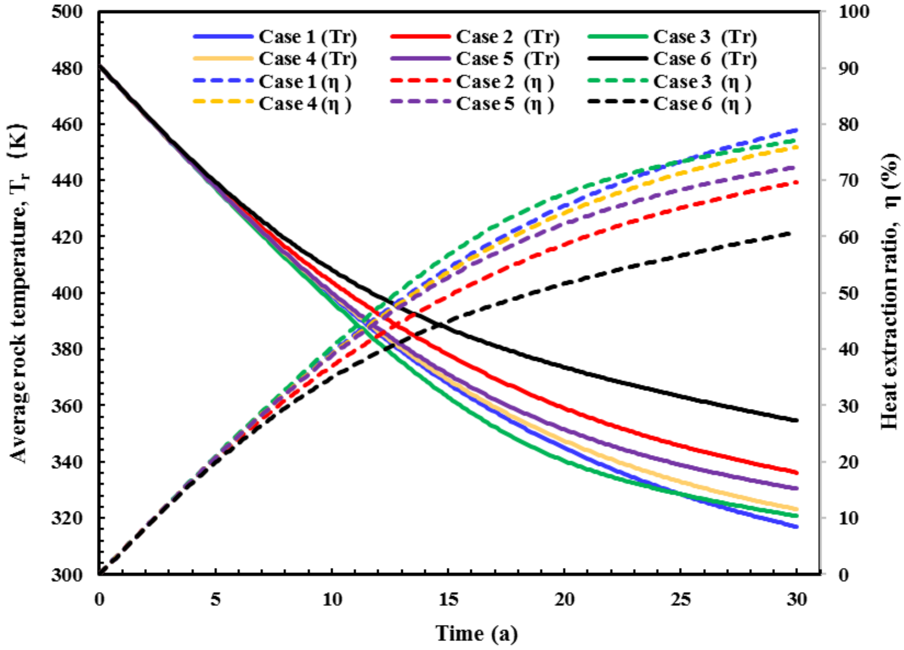

Figure 18. Average rock temperature and heat extraction ratio

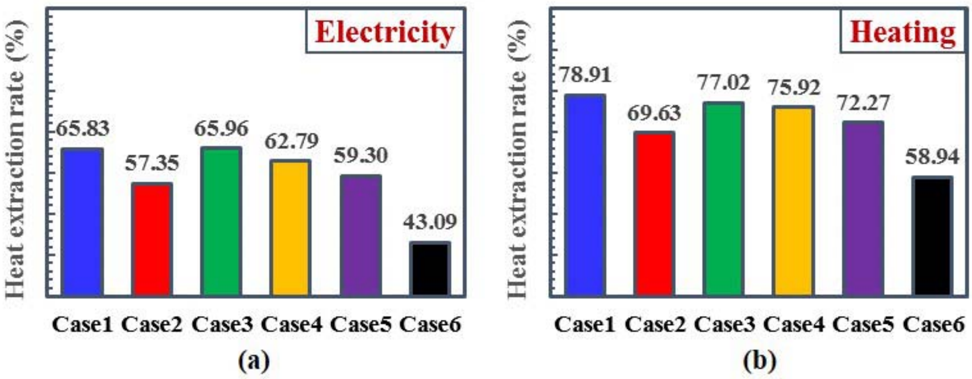

Figure 19. Heat extraction ratio for (a) Electricity generation and (b) Heating demand

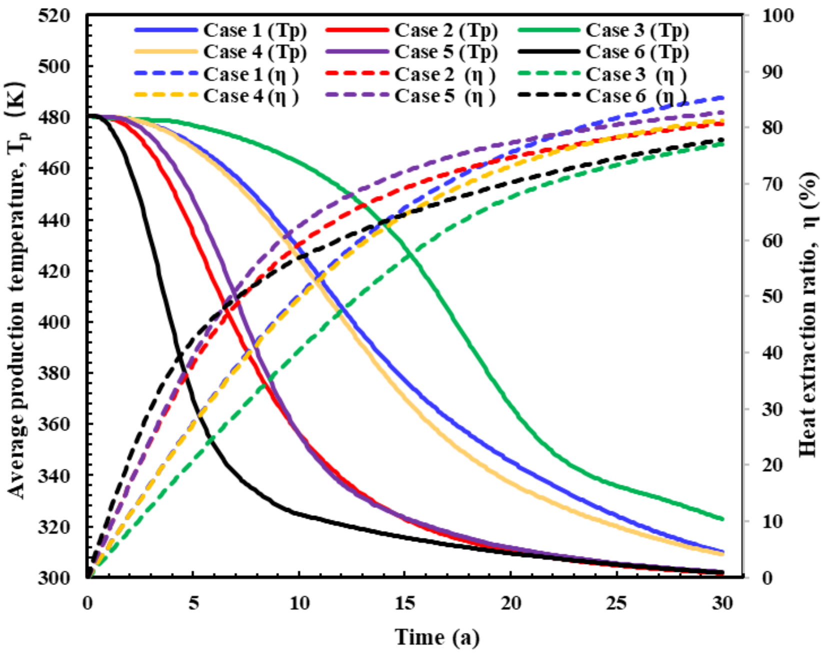

Figure 20. Average production temperature and heat extraction ratio under the single well injection mass flow rate is 40 kg/s

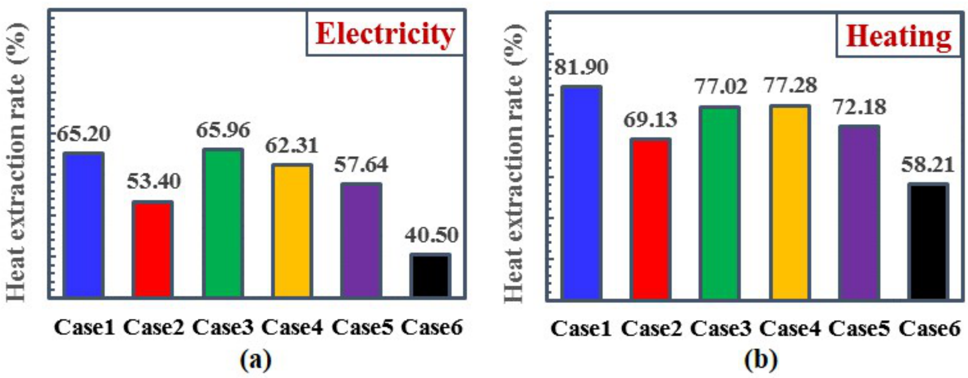

Figure 21. Heat extraction ratio for (a) Electricity and (b)Heating of different well layout under the single well injection mass flow rate is 40 kg/s

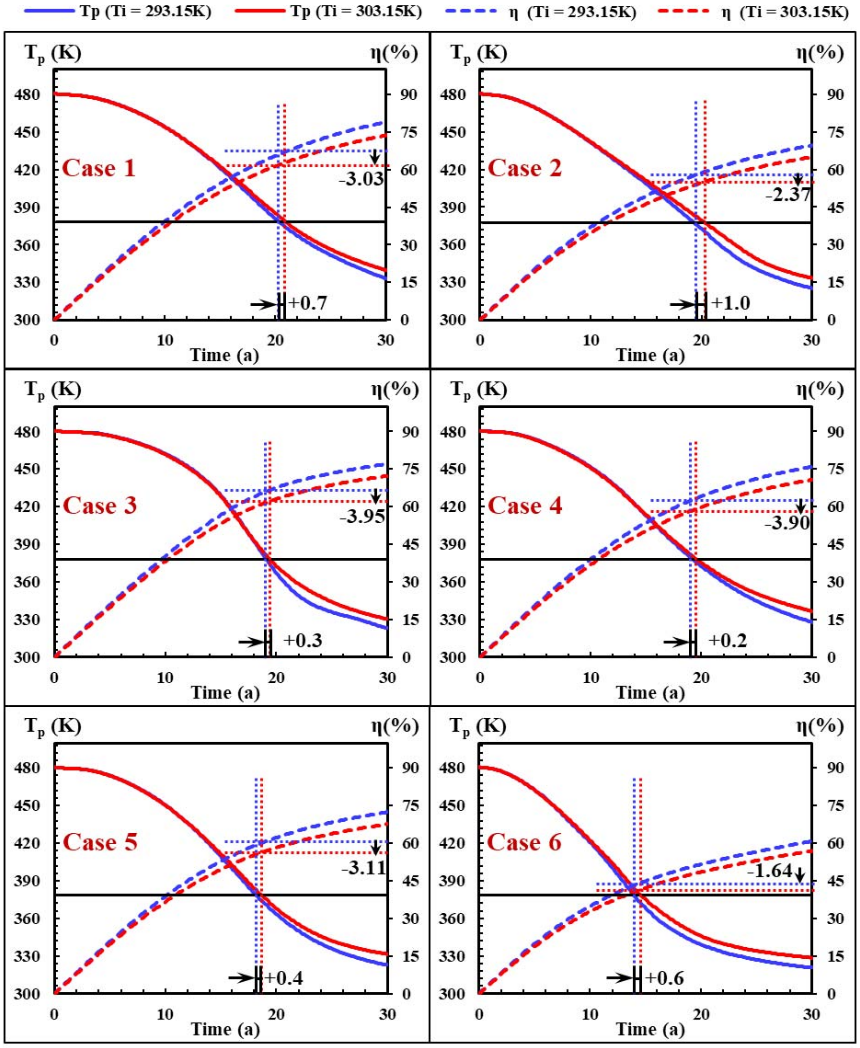

Figure 22. Comparison of average production temperature and heat extraction ratio under the injection temperature is 293.15 K and 303.15 K

Tables

Table 1. The reservoir descriptions of computational model

Description	HDR	Fracture	Unit
Density	2700	2000	kg/m^3
Porosity	0.08	1	%
Permeability	10e-15	10e-11	m^2
Heat conductivity	2.8	2.8	W/(m·K)
Heat capacity at constant pressure	1000	850	J/(kg·K)

Table 2. The spatial descriptions of computational model

Description	Case 1	Case 2	Case 3	Case 4	Case 5	Case 6

HDR dimensions	500m×500m×500m					
Injection well number	4	6	3	4	6	8
Production well number	2	2	1	1	1	1
Well diameter	1m	1m	1m	1m	1m	1m
Well length	500m	500m	500m	500m	500m	500m
Maximum well spacing	400m	400m	400m	400m	400m	400m
Fracture number	2	4	3	2	3	4
Fracture aperture	0.001m	0.001m	0.001m	0.001m	0.001m	0.001m
Fracture height	500m	500m	500m	500m	500m	500m

Table 3. The corresponding descriptions of initial and boundary conditions

Description	**Value**	**Unit**
Initial temperature at the top boundary	473.15	K
Geothermal gradient	0.03	K/m
Injection temperature	293.15	K
Initial pressure at the top boundary	40	MPa
Pressure gradient	0.005	MPa/m
Production pressure	30	MPa
Injection mass flow rate	120	kg/s

Table 4. Mesh of different well layout

Description	**Case 1**	**Case 2**	**Case 3**	**Case 4**	**Case 5**	**Case 6**
Minimum element quality	0.2139	0.1901	0.1956	0.212	0.149	0.1835
Average element quality	0.6379	0.636	0.6406	0.6394	0.6344	0.6381
Tetrahedron	137218	184761	102601	123124	154738	220493
Triangle	14072	24628	14254	15034	19514	29664
Edge element	1102	1540	912	972	1341	1685
Vertex element	28	40	28	18	34	34